STUDY OF IRREGULAR ROUGHNESS IN MINIMAL CHANNELS

J. Yang[1], A. Stroh[1], S. Jakirlić[2], B. Frohnapfel[1] and P. Forooghi[3,*]

[1]*Institute of Fluid Mechanics, Karlsruhe Institute of Technology, Karlsruhe, Germany*
[2]*Institute of Fluid Mechanics & Aerodynamics, Technical University Darmstadt, Darmstadt, Germany*
[3]*Dept. Mechanical & Production Engineering, Aarhus University, Aarhus, Denmark*

Abstract

Direct numerical simulation (DNS) is carried out to study turbulent flow over irregular rough surfaces in the periodic minimal channel. A passive scalar is presented in the flow to study heat transfer over rough surfaces with the Prandtl number $Pr = 0.7$. The generation of irregular roughness is based on a mathematical random algorithm, in which the power spectrum (PS) of the roughness height function along with its probability density function (PDF) can be directly prescribed. The hydro- and thermodynamic properties of the roughness, particularly the roughness function (ΔU^+) as well as the temperature profile offset ($\Delta\Theta^+$), are compared with those obtained from full span DNS for 6 types of roughness topographies with systematically varied PDF and PS configuration at $Re_\tau \approx 500$. The comparison confirms the capability of the minimal channel approach for characterization of irregular rough surfaces providing excellent agreement (within 5%) in ΔU^+ and $\Delta\Theta^+$ across various types of roughness topographies. Results also indicates that random realizations of roughness, with a fixed PS and PDF, translate to similar prediction with a narrow scatter. Finally, the impact of systematically varied roughness PDF and PS to both velocity and temperature profile is shown. It is also demonstrated that the influence of varying PDF and PS for roughness skin friction and heat transfer are different.

1 Introduction

Rough surfaces are abundant in nature (e.g. river beds and complex terrain) and engineering (e.g. degraded turbine blades, fouled ship hulls and iced aircraft surfaces). It is well established that the topography of roughness can significantly affect its hydrodynamic properties. In practice, the most important hydrodynamic effect of roughness is an increase in the skin friction coefficient of the surface. This increase manifests itself in a downward shift in the logarithmic region of inner scaled mean velocity profile ΔU^+. The shifted velocity profile in logarithmic layer

writes:

$$U^+ = \frac{1}{\kappa} \log(y^+) + A_m - \Delta U^+ . \tag{1}$$

Where $\kappa_m \approx 0.4$ is the von Karman constant, A_m is the smooth-wall offset. It is widely reported that ΔU^+ is related to the equivalent sand-grain roughness k_s (Jiménez 2004). the latter parameter is widely used as an input to engineering applications. Furthermore, $\Delta U^+ = \sqrt{2/C_{fs}} - \sqrt{2/C_{fr}}$ gives direct relation between roughenss function and skin friction (Schultz & Flack 2009), where C_{fs}, C_{fr} are the skin friction coefficients for smooth and rough wall at matched Re_τ respectively. Therefore, the central importance of this mean velocity downward shift ΔU^+ in determining the hydrodynamic property of the roughness is understood, which is referred to as the (Hama) roughness function. To find ΔU^+ for an arbitrary roughness at a certain roughness flow regime, one needs to either run a laboratory (or high-fidelity numerical) experiment or use a so-called roughness correlation, which relates the topography of roughness to ΔU^+. While the latter option is obviously less costly, large number of topographical metrics should be systematically investigated to construct such a predictive correlation e.g. skewness $Sk = (1/k_{\mathrm{rms}}^3) \int_S (k - k_{\mathrm{md}})^3 \mathrm{d}S$ and $k_{\mathrm{rms}} = \sqrt{(1/S) \int_S (k - k_{\mathrm{md}})^2 \mathrm{d}S}$ (Flack & Schultz 2010), effective slope ES$= (1/S) \int_S |\partial k/\partial x| \mathrm{d}S$ (Napoli *et al.* 2008), roughness correlation length L_{corr} (Sigal & Danberg 2008).

Similar to the skin friction, roughness can enhance the heat transfer of the surface, designed roughness are often used in engineering applications (Forooghi *et al.* 2017a). However, it is widely understood that the enhancement of heat transfer is not directly proportional to the increase of skin friction due to the lack of pressure-drag analog (Dipprey & sabersky 1963). This is reflected by the term 'Reynolds analogy factor' $RA = 2St/C_f$ (Bons 2005). Temperature profile of a forced convection smooth-wall flow is demonstrated also exhibits a logarithmic region (Kader 1981). The enhancement of heat transfer would result in a downward shift of this logarithmic temperature profile. Analogous to the Eqn. 1 The rough wall

---

temperature profile writes:

$$\frac{\Theta - \Theta_w}{\Theta_\tau} = \frac{1}{\kappa_h} \log(y^+) + A_h(Pr) - \Delta\Theta^+ , \quad (2)$$

where Θ represents the double-averaged temperature field, the offset A_h depends on the molecular Pandtl number $Pr \equiv \nu/\alpha$, α is the thermal diffusivity, Θ_w is the temperature at wall, Θ_τ is the friction temperature $\Theta \equiv (q_w/\rho c_p)/U_\tau$. q_w is the temporally and spatially averaged wall heat flux and c_p is the specific heat at constant pressure. Thus, the augmentation of heat transfer of a rough wall can be characterized by an analogous term to the roughness function ΔU^+, i.e. $\Delta\Theta^+$. The heat transfer coefficient of a rough surface, C_{hr}, can be derived by $\Delta\Theta^+$ with know C_{fr} at matched Re_τ through (MacDonald *et al.* 2019):

$$\begin{aligned}\Delta\Theta^+ = &\sqrt{\frac{C_{fs}}{2}} \Big(\frac{1}{C_{hs}} - \frac{1}{\kappa_m \kappa_h}\Big) \\ &- \sqrt{\frac{C_{fr}}{2}} \Big(\frac{1}{C_{hr}} - \frac{1}{\kappa_m \kappa_h}\Big) .\end{aligned} \quad (3)$$

It is since long desired for *a priori* prediction of the aforementioned quantities to get rid of resource demanding (numerical) experiments. Flack proposed use of Direct Numerical Simulation (DNS) for generating massive database needed for a universal roughness correlation (Flack 2018). The major problems in reaching this goal are a) the computational cost of DNS and b) the measurements of realistic rough surfaces are rare and not suitable for systematic studies. The aim of this work is to examine a new framework, which overcomes both obstacles. To relieve the computational cost we simulate the flow in fully developed turbulent channels with reduced streamwise and spanwise sizes. The idea was previously established and validated by Chung *et al.* (2015), MacDonald *et al.* (2016, 2019) with sinusoidal roughness structure. The criteria of the minimal channel size is given by the authors: $L_z^+ \geq \max(100, \tilde{k}^+/0.4, \lambda_{\sin}^+)$, $L_x^+ \geq \max(1000, 3L_z^+, \lambda_{\sin}^+)$. Where L_x and L_z are the streamwise and spanwise extend of the channel, respectively, $\tilde{k}$ is the amplitude of the sinusoidal structure. $\lambda_{\sin}$ represents the wavelength of the sinusoidal structure. The criteria are set with the aim of accommodating the minimal channel to the near wall turbulence as well as the roughness structure. The research shows that minimal channel following the criteria above is capable for this type of roughness (repetitive) structure to predict the roughness function ΔU^+ as well as the temperature offset $\Delta\Theta^+$, but has not been examined for irregular roughness up to now, i.e. the effect of repeating irregular roughness and the limited sample size of roughness topography introduced by the significantly reduced spanwise extend of minimal channel is yet unknown.

In order to evaluate the validity of this approach for irregular rough surfaces we employ the random algorithm proposed by Pérez-Ràfols & Almqvist (2019). With the roughness generation method surface is generated randomly while the roughness statistical properties can be controlled by its height probability density function (PDF) and the power spectrum (PS) (hence the term pseudo-random roughness). The generation process is realized by discrete fast Fourier transform (DFFT), thus it is inherently suitable for the DNS simulations where periodic boundary condition is required.

In the present work, pseudo-random roughness with different prescription of PDF and PS are generated and simulated in both minimal channels and conventional full-span channels at $Re_\tau \approx 500$. The performance of the roughness generation method as well as the minimal channels are demonstrated. The impact of different roughness height PDF and PS configurations on both velocity and temperature fields is exhibited.

2 Methodology

Pseudo-random roughness generation method

The pseudo-random roughness is generated with the method originally proposed by Pérez-Ràfols & Almqvist (2019), which will be referred to as generation method for the following text. The roughness structure function k is represented by discrete elevation map on 2-D Cartesian grid, i.e. $k(x, z)$, where x, z are the streamwise and spanwise coordinate respectively. Initially, a roughness map with prescribed roughness PDF is given and is labeled as k_{PDF}^0. This map do not necessarily contain desired PS. For the next step, this map is transformed using DFFT and compared with the second initial map with desired PS, which is labeled as k_{PS}^0. After that, the field is transformed back with inverse DFFT and adjust the height distribution to fit the PDF. The iterative adjustment of PDF and PS continues until the error, which are measured by the percentage disagreement of PDF and PS profile respectively, approaches a stationary low value. For further information readers are referred to the literature (Pérez-Ràfols & Almqvist 2019).

Direct numerical simulation

Direct numerical simulations are carried out in fully developed turbulent channels. Flow is driven by constant pressure gradient P_x. Periodic boundary condition is applied to the streamwise and spanwise boundaries of the channel. Upper and lower wall are roughened by the roughness structures. The roughness with no-slip &

zero-temperature boundary condition is realized by imposing immersed boundary method (IBM) following Goldstein's method (Goldstein 1993). Where negative external force is applied to the flow in the roughness elements to obtain zero velocity & temperature inside the roughness. An source term $Q = \mathbf{u}$ is added to the temperature field to obtain a steady temperature field as the flow flowing through periodic channel and being cooled by the zero-temperature roughness boundaries. Thus, the Navier-Stokes equation writes:

$$\nabla \cdot \mathbf{u} = 0 \, , \tag{4}$$

$$\frac{\partial \mathbf{u}}{\partial t} + \nabla \cdot (\mathbf{u}\mathbf{u}) = -\frac{1}{\rho}\nabla p + \nu \nabla^2 \mathbf{u} - \frac{1}{\rho}P_x \hat{\mathbf{e}}_{\mathbf{x}} + \mathbf{F}_u \, , \tag{5}$$

$$\frac{\partial \theta}{\partial t} + \nabla \cdot (\mathbf{u}\theta) = \alpha \nabla^2 \theta + Q + \mathbf{F}_\theta \, , \tag{6}$$

where $\mathbf{u}$ is the velocity vector $\mathbf{u} = (u, v, w)^\intercal$, P_x is the mean pressure gradient in the flow direction added as a constant and uniform source term to the momentum equation to drive the flow in the channel. Here p, $\hat{\mathbf{e}}_{\mathbf{x}}$, ρ, ν, $\mathbf{F}_\theta$ and $\mathbf{F}_u$ are pressure fluctuation, Kronecker delta, density, kinematic viscosity and external source term for momentum and energy equation due to IBM, respectively. The Friction Reynolds number is defined as $Re_\tau = u_\tau(H - k_{\mathrm{md}})/\nu$, where $u_\tau = \sqrt{\tau_w}$ is the friction velocity and $\tau_w = -P_x(H - k_{\mathrm{md}})$ is the wall shear stress controlled by the constant pressure gradient.

Description of cases

Thanks to the flexibility of the roughness generation method, two of the roughness parameters chosen from both PDF and PS sides are systematically varied and analyzed utilizing DNS, namely Sk and the PS slope p. Three values of Sk are selected i.e. $Sk \approx -0.48, 0, 0.48$. Skewed roughness distribution obeys Weibull's distribution $f(k) = K\beta^K k^{(K-1)}e^{-(\beta k)^K}$, where K is the form factor which is adjusted to match desired Sk, non-skewed roughness obeys the Gaussian distribution $f(k) = e^{-\frac{1}{2}(\frac{k-\mu}{\sigma})^2}/(1/\sigma\sqrt{2\pi})$. Moreover the kurtosis $Ku \approx 3$ is selected for all roughness in search of the similarity to the Gaussian distribution. Therefore, the PDF are characterized in terms of negatively skewed, Gaussian and positively skewed distribution. The height of the roughness is scaled by the the 99% confidence interval of the PDF, which is denoted as k_{99}. $k_{99} = 0.1H$ is prescribed to all roughness configurations. In order to avoid extreme high/low roughness, roughness elements locate out side $1.2 \times k_{99}/2$ around the meltdown height $k_{md} = (1/S)\int_S k\mathrm{d}S$ are excluded, where S is the wall-normal projection area of the surface.

On the other side, power-law PS is employed, i.e. $E_k(\mathbf{q}) = C_0(\|\mathbf{q}\|/q_0)^p$, where $\mathbf{q}$ is the

wavenumber vector $\mathbf{q} = (q_x, q_z)^\intercal$, $q_0 = 2\pi/\lambda_0$ is the referencing wavenumber corresponding to the largest in-plane length scale λ_0, C_0 is a constant to scale the roughness height, and p is the slope of the power-law PS. p is chosen as -1 and -2 in seek of overlapping with previous researches (Barros *et al.* 2018, Nikora *et al.* (2019)). The cutoff wavelengths of the PS are selected to be moderate to the channel size as well as the grid resolution, i.e. the presenting roughness wavelength λ obeys $0.8H \leq \lambda \leq 0.08H$.

In summary, by "grid searching" of these two roughness parameters in two channel sizes, in total 12 ($3 \times 2 \times 2$) rough surfaces are individually produced. Following abbreviation is used throughout the text to distinguish the cases:

$$\underbrace{\overbrace{\boxed{G}}^{\text{Topography}}\underbrace{\boxed{2}}_{-p}}_{\text{PDF}} \mid \overbrace{\boxed{F}}^{\text{Channel size}} \quad . \tag{7}$$

- The first character indicates the type of PDF; G for Gaussian distribution, P for positively skewed ($Sk \approx 0.48$), and N for negatively skewed ($Sk \approx -0.48$).

- The second digit indicates the PS slope; 1 for $p = -1$ and 2 for $p = -2$.

- The following character(s) indicates the channel size; F for full channel ($8H \times 4H$), M for the minimal channel ($2.4H \times 0.8H$)

One of the irregular roughness topographies, $G2F$, is illustrated in figure 1, the size of the minimal channel is represented by the black frame in the figure. The roughness metrics that are widely used for roughness characterization are shown in Table 1. As one can see, the roughness topographical statistics from the random generation process are preserved for both surface sizes. It is worth mentioning that the roughness for minimal channels and full span channels are independently generated, which means each surface has an individual realization but the statistics are controlled by the generation method. Thus, the stability of the generation method is demonstrated in terms of roughness topographical statistics.

3   Results

The DNS results, especially the mean velocity and temperature profiles, $\langle\overline{u}\rangle(y)$ and $\langle\overline{\theta}\rangle(y)$ are obtained by applying double-averaging method: $\langle\overline{\Phi}\rangle(y) = \frac{1}{S}\iint_S \overline{\Phi}(x, y, z)\mathrm{d}x\mathrm{d}z$. Where $\overline{\Phi}(x, y, z)$ is the time averaged velocity $\overline{u}$ /temperature $\overline{\theta}$ field. The angular bracket $\langle\cdot\rangle$ denotes horizontal averaging. The double-averaged velocity and temperature profiles will be denoted as U and Θ, respectively.

Topography	Sk	p	k_{md}/H	k_{rms}/H	L_x^{corr}/H	S_f/S	ES	ΔU^+	$\Delta\Theta^+$
$P1F$	0.48	-1	0.046	0.0208	0.052	0.28	0.57	7.33	4.70
$P1M$	0.48	-1	0.046	0.0208	0.056	0.28	0.55	7.28	4.72
$P2F$	0.48	-2	0.046	0.0208	0.100	0.21	0.44	6.99	3.93
$P2M$	0.48	-2	0.046	0.0208	0.110	0.20	0.40	6.86	4.37
$G1F$	0	-1	0.061	0.0200	0.050	0.27	0.54	6.67	3.93
$G1M$	0	-1	0.061	0.0200	0.054	0.27	0.53	6.66	3.99
$G2F$	0	-2	0.061	0.0200	0.100	0.20	0.43	6.30	3.62
$G2M$	0	-2	0.061	0.0200	0.108	0.19	0.40	6.39	3.70
$N1F$	-0.48	-1	0.074	0.0208	0.052	0.28	0.57	6.14	4.73
$N1M$	-0.48	-1	0.074	0.0208	0.056	0.28	0.55	6.07	4.68
$N2F$	-0.48	-2	0.074	0.0208	0.100	0.21	0.44	5.82	4.44
$N2M$	-0.48	-2	0.074	0.0208	0.110	0.20	0.40	5.63	4.38

Table 1: Roughness topographical statistics, where S_f is the total frontal projected area of the roughness. L_x^{corr} refers to the length scale where the roughness auto-correlation in streamwise direction drops under 0.2. Simulation results are shown on the last two columns on the left.
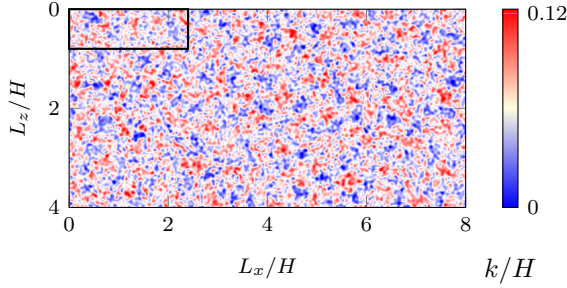

Figure 1: Full-span roughness sample $G2F$. The black rectangle represents the size of the minimal channel. Color bar shows the surface height.

Figure 2: Mean velocity profile of roughness type $G2$, dashed line: velocity profile of smooth wall U_s^+, solid line: velocity profile of rough wall U_r^+. The inset shows the velocity retardation $U_s^+ - U_r^+$ as a function of wall normal distance $(y-d)^+$.

Furthermore, due to the fluctuating surface structure the origin of the wall normal coordinate of a rough surface cannot be naturally defined. In order to align the logarithmic layer of smooth and rough surfaces, zero plane displacement d is considered. To this end, Jackson (1981) proposed use of moment centroid of the drag profile on rough surfaces as the virtual origin for the logarithmic velocity profile. The definition of the zero plane displacement d in present work follows Jackson's method.

Effect of channel size

The velocity field of exemplary cases $G2M$ and $G2F$ are compared in figure 2. The velocity offset profiles $U_s^+ - U_r^+$ are shown in the inset of figure 2 using same coloring style. With the same measurement, temperature fields predicted by minimal channel and full span channel are compared in figure 3. As one can observe, excellent agreement of the profiles are achieved between minimal channels and full span channels below each critical height y_c. Due to the nature of minimal channels, sudden increase of the profiles
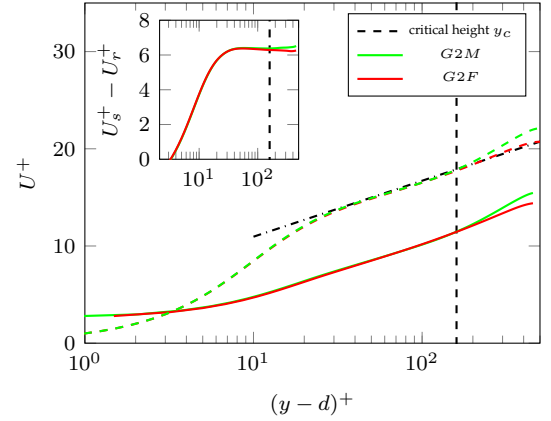
in outer layer can be observed for both smooth and rough cases. However, the offset profiles of minimal channel and full span channel, as shown in the inset, collapse well and reach constant values in logarithmic layer. The roughness function ΔU^+ as well as $\Delta\Theta^+$ are obtained by measuring the mean offset of the profile in logarithmic layer, specifically over $y^+ = 160 - 250$.

Generalizing the observation to all considered cases, ΔU^+ along with $\Delta\Theta^+$ are summarized on the last two columns in table. 1. To visualize the disagreement of minimal channel with full span channel, graphical comparison are illustrated in figure 4. It can be observed that minimal channels show excellent agreement with the conventional full span channels, the discrepancies of both ΔU^+ and $\Delta\Theta^+$ lie under 5%. Consistent predictions in-
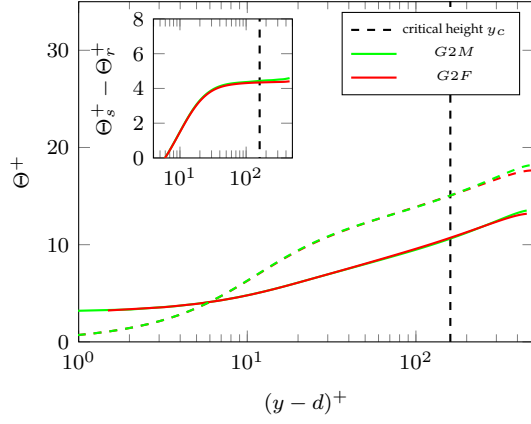
Figure 3: Mean temperature profile of roughness type $G2$, dashed line: temperature profile of smooth wall Θ_s^+, solid line: temperature profile of rough wall Θ_r^+. The inset shows the temperature retardation $\Theta_s^+ - \Theta_r^+$ as a function of wall normal distance $(y-d)^+$.
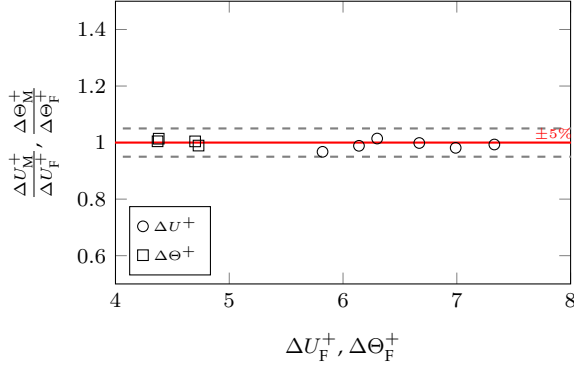

Figure 4: ΔU_M^+ and $\Delta\Theta_M^+$ predicted by minimal channels normalized by full span channel prediction ΔU_F^+ and $\Delta\Theta_F^+$, respectively ∘: ΔU^+, □: $\Delta\Theta^+$. Gray dashed lines indicate the boundary of 5% error interval around $\Delta U_M^+/\Delta U_F^+ = \Delta\Theta_M^+/\Delta\Theta_F^+=1$

dicate the capability of the minimal channels in reproducing the hydro- and thermodynamic properties of the irregular pseudo-realistic roughness. The results imply the determining characters of the roughness PS and PDF to both skin friction and heat transfer.

Effect of roughness topography

Given the satisfactory performance of minimal channel simulations, in the following content the prediction results by minimal channels will be analysed. An overview of the roughness function ΔU^+ from minimal channel simulations is plotted in figure 5, where roughness function ΔU^+ is shown as a function of skewness Sk, grouped by the PS slope p. As investigated by Flack *et al.*(2020), positively skewed rough surfaces give higher skin friction than non-skewed or
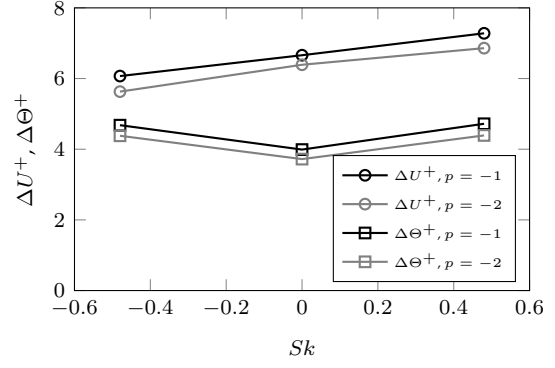

Figure 5: ΔU^+(circles) and $\Delta\Theta^+$(squares) predictions from minimal channels. Black: $p = -1$, gray: $p = -2$.
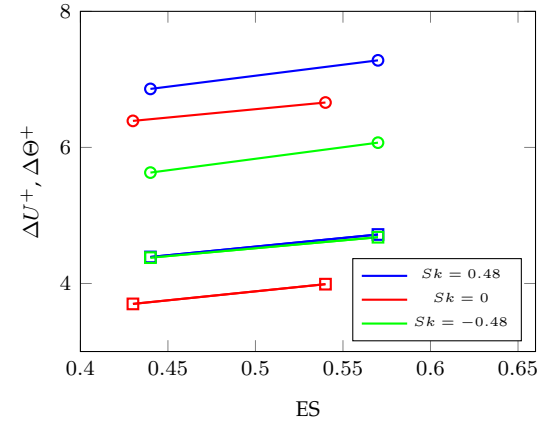

Figure 6: ΔU^+(circles) and $\Delta\Theta^+$(squares) predictions from minimal channels. Blue: $Sk = 0.48$, red: $Sk = 0$, green: $Sk = -0.48$.

negatively skewed roughness. Negatively skewed surfaces show 'slip-velocity' effect (Jelly & Busse 2018), which translates into a weaker mean velocity retardation. The trend observed in the present results fully agrees with what suggested by the previous researchers.

On the other hand, the averaged offset of logarithmic temperature profile $\Delta\Theta^+$, analogous to ΔU^+, are shown in figure 6. The evolution of $\Delta\Theta^+$ show significant difference to ΔU^+ – both in value and trend. It is demonstrated that Gaussian surfaces show lowest interference to temperature field while these skewed roughness, regardless of its sign, can enhance the temperature offset. By adjusting the PS slope p the shift of $\Delta\Theta^+$ can be observed for all roughness topographies. To shed light into the correlation of spatial roughness distribution and $\Delta\Theta^+$, $\Delta\Theta^+$ is plotted as a function of effective slope ES in figure 6. Approximately parallel increases of $\Delta\Theta^+$ with ES for all types of roughness are exhibited. Similar trend can be found for ΔU^+. Notably, surfaces whose $Sk = \pm0.48$ show comparable value of $\Delta\Theta^+$. The
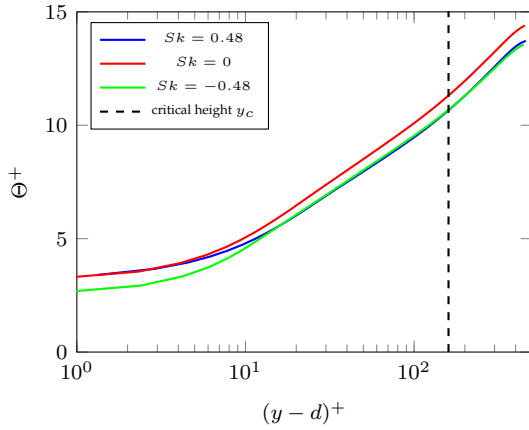
Figure 7: Temperature profiles of $G/P/N2M$

exemplary temperature profiles of $P2M$, $G2M$ and $N2M$ are ploted in figure 7. In the near wall region, due to the different blockage effect introduced by skewness, temperature profiles diverge. However in the logarithmic layer, the temperature profiles of positively and negatively skewed roughness collapse. Have to mention that identical $\Delta\Theta^+$ of negatively and positibely skewed roughness do not necessarily translate to a identical C_{hr} according to Eqn. **??**. Detailed study of the effect of skewness on the heat transfer coefficient should be carried out.

4   Conclusions

DNS is carried out for fully developed turbulent flow over artificial irregular roughness driven by constant pressure gradient at $Re_\tau \approx 500$. A source term for temperature field is applied while the temperature for the roughness is prescribed to be 0. The rough surfaces are generated based on the mathematical roughness generation method proposed by Ràfols & Almqvist(2019). With the generation method roughness with desired PDF and PS can be generated. 3 types of PDF, namely $Sk = -0.48, 0, 0.48$ are combined with 2 types of power-law PS inputs whose slope $p = -1\& -2$. First of all, the performance of the roughness generation method is assessed by showing the statistics of independently generated surfaces for full span channel and minimal channel. It is demonstrated that the minimal channel is capable for reproducing the hydro- and thermodynamic properties of the artificial irregular roughness with significant reduction of computational effort. In the present work, roughness function ΔU^+ and the offset of temperature profile in logarithmic layer ΔT^+ are compared among all types of roughness topographies with systematically adjusted PDF and PS. It is found that the influence of roughness is different for skin friction and heat transfer. A

monotonically increase of ΔU^+ as a function of Sk is observed, while for temperature field the skewed roughness – regard less peak or pit dominant – can enhance the heat transfer to an comparable extent relative to non-skewed roughness with identical PS. General increase of ΔU^+ and $\Delta\theta^+$ is reported when the PS slope p is steeper. Parallel increase of skin friction and heat transfer for different types of roughness can be observed with increasing ES.

References

Jiménez, J. (2004), Turbulent flows over rough walls, *Ann. Rev. Fluid Mech.* Vol. 36, pp. 173-196.

Flack, K. A. (2018), Moving beyond Moody, *J. Fluid Mech.*, Vol. 842, pp. 1-4.

Chung, D., Chan, L., MacDonald, L., Hutchins, N. and Ooi, A. (2015), A fast direct numerical simulation method for characterising hydraulic roughness, *J. Fluid Mech.*, Vol. 773, pp. 418-431.

Pérez-Ràfols, F. and Almqvist, A. (2019), Generating randomly rough surfaces with given height probability distribution and power spectrum, *Tribology International*, Vol. 131, pp. 591-604.

Flack, K. A. and Schultz, M. P. (2010), Review of Hydraulic Roughness Scales in the Fully Rough Regime, *J. Fluids Engineering*, Vol. 132.

Napoli, E., Armenio, V. and De Marchis, M (2008). The effect of the slope of irregularly distributed roughness elements on turbulent wall-bounded flows, *J. Fluid Mech.*, Vol. 613. pp. 385-394.

MacDonald, M., Chung, D. Hutchins, N., Chan, L., Ooi, A. and García-Mayoral, A. (2016), The minimal channel: a fast and direct method for characterising roughness, *Journal of Physics: Conference Series*, Vol. 708,

Sigal, A., Danberg, J. E. (2008), New correlation of roughness density effect on the turbulent boundry layer, *AIAA Journal*, Vol. 28, pp. 554-556.

Goldstein, D., Handler, R. and Sirovich, L., Modeling a no-slip flow boundary with an external force field., *Journal of Computational Physics*, Vol. 105, pp. 354-366.

Forooghi, P., Flory, M., Bertsche, D., Wetzel, T. and Frohnapfel, B. (2017a). Heat transfer enhancement on the liquid side of an industrially designed flat-tube heat exchanger with passive insertes-numerical investigation. *Appl. Therm. Eng.*, Vol. 123, pp. 573-583.

Bons, J.P. (2005) A critical assessment of Reynolds analogy for turbine flows. *ASME J. Heat Transf.*, Vol. 127(5), pp. 472-485.

Kader, B. A. (1981) Temperature and concentration profiles in fully turbulent boundary layers. *Intl. J. Heat Mass Transfer*, Vol. 24, pp. 1541-1544.

Cebeci, T. and Bradshaw, P. (1984), Physical and computational aspects of convective heat transfer. Springer.

MacDonald, M., Hutchins, N., Chung, D. (2019), Roughness effects in turbulent forced convection, *J. Fluid Mech.*, Vol. 861, pp. 138-162.

Barros, J. M., Schultz, M. P. and Flack, K. A. (2018), Measurements of skin-friction of systematically generated surfaces roughness,*Intl. J. Heat and Fluid Flow*, Vol. 72, pp. 1-7.

Nikora, V. I., Stoesser, T., Cameron, S. M., Stewart, M., Papadopoulos, K., Ouro, P., McSherry, R.,Zampiron, A., Marusic, I., Falconer, R. A. and et al (2019), Friction factor decomposition for rough-wall flows: theoretical background and application to open-channel flows, *J. Fluid Mech.*, Vol. 872, pp. 626-664.

Flack, K.A., Schultz. M.P. & Barros, J.M. 2020 Skin friction measurements systematically-varied roughness: Probing the role of roughness amplitude and skewness. *Flow, Turbulence and Combustion*, Vol. 104, pp.317-329.

Jelly, T.O. & Busse, A. 2018 Reynolds and dispersive shear stress contributions above highly skewed roughness *J. Fluid Mech.* vol. 852, pp. 710-724.

Jackson, P.S. 1981 On the displacement height in the logarithmic velocity profile. *J. Fluid Mech.* vol.111, pp.15-25.